

Discovering Potassium Channel Blockers from Synthetic Compound Database by Using Structure-Based Virtual Screening in Conjunction with Electrophysiological Assay

Hong Liu,[†] Zhao-Bing Gao,[†] Zhiyi Yao,[†] Suxin Zheng, Yang Li, Weiliang Zhu, Xiaojian Tan, Xiaomin Luo, Jianhua Shen, Kaixian Chen, Guo-Yuan Hu,* and Hualiang Jiang*

Center for Drug Discovery and Design, State Key Laboratory of Drug Research, Shanghai Institute of Materia Medica, Shanghai Institutes for Biological Sciences, Chinese Academy of Sciences, 555 Zu Chong Zhi Road, Zhangjiang Hi-Tech Park, Shanghai 201203, P. R. China

Received April 10, 2006

Potassium ion (K^+) channels are attractive targets for drug discovery because of the essential roles played in biological systems. However, high-throughput screening (HTS) cannot be used to screen K^+ channel blockers. To overcome this disadvantage of HTS, we have developed a virtual screening approach for discovering novel blockers of K^+ channels. On the basis of a three-dimensional model of the eukaryotic K^+ channels, molecular docking-based virtual screening was employed to search the chemical database MDL Available Chemicals Directory (ACD). Compounds were ranked according to their relative binding energy, favorable shape complementarity, and potential to form hydrogen bonds with the outer mouth of the K^+ channel model. Twenty candidate compounds selected from the virtual screening were examined using the whole-cell voltage-clamp recording in rat dissociated hippocampal neurons. Among them, six compounds (5, 6, 8, 18–20) potently blocked both the delayed rectifier (I_K) and fast transient K^+ currents (I_A). When applied externally, these six compounds preferentially blocked I_K with potencies 2- to 500-fold higher than that of tetraethylammonium chloride. Intracellular application of the six compounds had no effect on both K^+ currents. In addition, the interaction models and binding free energy calculations demonstrated that hydrophobic interaction and solvent effects play important roles in the inhibitory activities of these compounds. The results demonstrated that structure-based computer screening strategy could be used to identify novel, structurally diverse compounds targeting the pore binding pocket of the outer mouth of voltage-gated K^+ channels. This study provides an alternative way of finding new blockers of voltage-gated K^+ channels, while the techniques for high-throughput screening of K^+ channel drugs remain in development.

1. Introduction

Potassium ion (K^+) channels consist of a ubiquitous family of membrane proteins that play critical roles in a wide variety of physiological processes, such as the regulation of neuronal excitability, muscle contraction, cell proliferation, and insulin secretion.¹ The abundant diversity for structures and functions of K^+ channel family members is supported by sequencing studies of the *Caenorhabditis elegans* genome. About 100 unique K^+ channels genes have been predicted to exist in this organism.^{2,3} Mammalian K^+ channels are classified into three groups in terms of their membrane topology: (1) voltage-gated K^+ channels (Kv) and Ca^{2+} -activated K^+ channels, which contain six transmembrane domains (TMDs); (2) “leak” K^+ channels, which have four TMDs; (3) inward-rectifier K^+ channels (Kir), which contain two TMDs.⁴ Each K^+ channel group consists of multiple subfamily members. Impaired functions of K^+ channel or mutations in the genes encoding K^+ channels have been demonstrated to cause a wide spectrum of human diseases.^{5,6}

In addition to the substantial advances in molecular cloning and functional studies of K^+ channels, the structural elucidation of K^+ channels has rapidly progressed. Thus far, the crystal structures of four bacterial homologues of different mammalian K^+ channels have been elucidated using X-ray analysis. They are (1) KcsA, a pH-gated K^+ channel from *Streptomyces*

lividans,^{7,8} (2) MthK, a Ca^{2+} -gated K^+ channel from *Methanobacterium thermoautotrophicum*,⁹ (3) Kv, a voltage-gated K^+ channel from *Aeropyrum pernix* and *Pichia pastoris*,^{10,11} and (4) KirBac, an inward rectifier K^+ channel from *Burkholderia pseudomallei*.¹² In general, the functional K^+ channels consist of four subunits (tetramer), and each subunit contributes two transmembrane α -helices (denoted M1 and M2 in KcsA, MthK, and KirBac and denoted S5 and S6 in Kv channels) plus a re-entrant loop, which forms the central K^+ -selective pore.^{13–15} The pore-forming regions of both prokaryotic and eukaryotic K^+ channels are highly conserved, including a pore-helix and an extended filter region that contains the TVGYG sequence motif.¹⁶ The structural biology studies clearly elucidate the molecular mechanisms underlying the K^+ conduction and selectivity,^{7–8,11,14} giving indisputable evidence that the ion permeation pathway across the membrane is indeed at the center of four identical subunits that cluster around the narrowest part of the pore formed by the P loop.^{7,8} Moreover, the existing crystal structures of K^+ channels also provide a solid framework for constructing three-dimensional (3D) model of the eukaryotic K^+ channels for drug discovery.

Structure-based virtual screening (SBVS) approaches based on molecular docking have become promising tools for discovering active compounds.^{17–22} We successfully constructed a three-dimensional model for the eukaryotic voltage-gated K^+ channels based on the crystal structure of KcsA channel from *Streptomyces lividans*⁷ and developed a computational virtual screening approach to search for new blockers of K^+ channels from large databases. Four candidate compounds discovered from the China Natural Products Database using SBVS were demonstrated to possess a potent K^+ channel blocking effect.

* To whom correspondence should be addressed. For G.-Y.H.: phone, +86-21-50806778; fax, +86-21-50807088; e-mail, gyhu@mail.shnc.ac.cn. For H.J.: phone, +86-21-50806600, extension 1303; fax, +86-21-50807088; e-mail, hljiang@mail.shnc.ac.cn.

[†] Equivalent contributors.

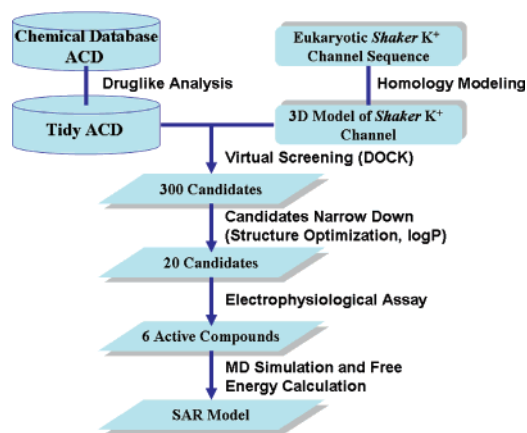


Figure 1. Computational and experimental flow chart for this study.

In rat hippocampal neurons they are 20–1000 times more potent than the classical delayed rectifier K^+ channel blocker tetraethylammonium chloride.²³ Continuing this study, we have recently used this approach to search for K^+ channel blockers from the synthetic compounds. In this study, we show that novel structurally diverse blockers of K^+ channels can be found in the large chemical database MDL Available Chemicals Directory (ACD)²⁴ using SBVS in conjunction with chemical synthesis and electrophysiological assay. Twenty candidate compounds were selected from the ACD database with relatively low binding energy, favorable shape complementarity, and/or potential to form hydrogen bonds with the K^+ channel. The electrophysiological assay demonstrated that six compounds showed potent blocking effects on voltage-gated K^+ channels in rat hippocampal neurons.

2. Materials and Methods

The computational and experimental flow chart is shown in Figure 1. Briefly, 300 candidate molecules were first selected from the ACD database by using the docking program DOCK4.0²⁵ targeting the binding site of a 3D model of the eukaryotic Shaker K^+ channel constructed by homology modeling. Before virtual screening, nondruglike molecules were filtered out from the ACD database using a druglike analysis filter developed by us.²⁶ Afterward, the binding models of the candidates with the K^+ channel were optimized using molecular mechanics, and $\log P$ values of the candidates were predicted using the XlogP program.²⁷ According to the DOCK scoring results, interaction models (shape complementarities between candidates and K^+ channel), and the XlogP values, 20 compounds were selected for bioassay. Six active compounds were discovered through electrophysiological screening. The binding models and binding free energies of the active compounds to the K^+ channel were re-estimated by using the MD simulation and MM/GBSA approach,²⁸ based on which structure–activity relationship of these active compounds was discussed. The details of the computations and experiments are described as follows.

2.1. Modeling and Computation. 2.1.1. 3D Model of Eukaryotic Shaker K^+ Channel. The 3D model of eukaryotic Shaker K^+ channels was generated on the basis of the crystal structure of the KcsA K^+ channel retrieved from the Brookhaven Protein Data Bank (PDB) (<http://www.rcsb.org/pdb/>) (entry 1BL8)⁷ using our previously reported procedure.²³ The sequences of eukaryotic Shaker K^+ and KcsA channels were obtained from the SwissProt database (entries P08510 and Q54397, respectively). A sequence alignment of KcsA and eukaryotic channels with the Shaker K^+ channels was carried

out by using the GCG software.²⁹ The side chains of residues Arg27, Ile60, Arg64, Glu71, and Arg117 missing in the current KcsA crystal structure were added using the Biopolymer module of Insight II.³⁰ The Biopolymer module of Insight II³⁰ was also used to construct the 3D structural model of eukaryotic Shaker K^+ channels by mutations of Pro55Glu (P55E), Ala57Ser (A57S), Ile60Lys (I60K), Thr61Ser (T61S), Arg64Asp (R64D), Leu81Met (L81M), and Tyr82Thr (Y82T) on the X-ray crystal structure of the KcsA K^+ channel.⁷ After a preliminary optimization of the side chains, the entire 3D model was minimized by 200 steps of steepest descent, followed by Powell minimization to a root-mean-square (rms) energy gradient of 0.05 kcal/(mol·Å). The AMBER force field with the Kollman all-atom charges^{31,32} was employed during the structural optimization. The quality of the model was checked by the Prostat program in Insight II.³⁰

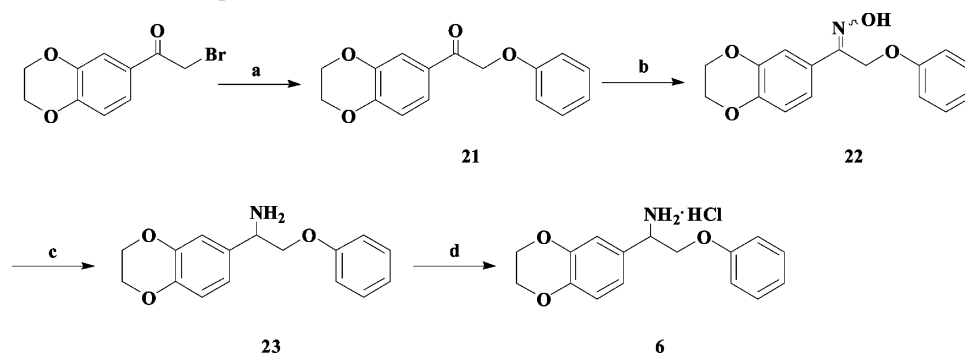
2.1.2. Virtual Screening. The ACD database containing the structural information of 200 000 chemicals (<http://www.mdll.com>)²⁴ was used for the virtual screening. A chemistry space filter for scoring druglikeness²⁶ developed in our laboratory was used to remove the nondruglike structures from the ACD. DOCK4.0²⁵ was employed for the primary screening. Residues around the motif TXXTVGYG of the K^+ channel at a radius of 5 Å were isolated for constructing the grids of docking screening. During the docking calculation, Kollman all-atom charges³¹ were assigned to the protein, and Gasteiger–Marsili charges³³ were assigned to the small molecules in the tidy ACD. The flexibility of each small molecule was considered during the virtual screening. The top 300 molecules were selected for further analysis.

The structures of the complexes of the K^+ channel with the DOCK selected molecules were optimized automatically by running a SPL program encoded into the Sybyl³² environment written by us to adjust the orientation and interaction. The binding energy (ΔE_{bind}) between each molecule and K^+ channel was calculated by using

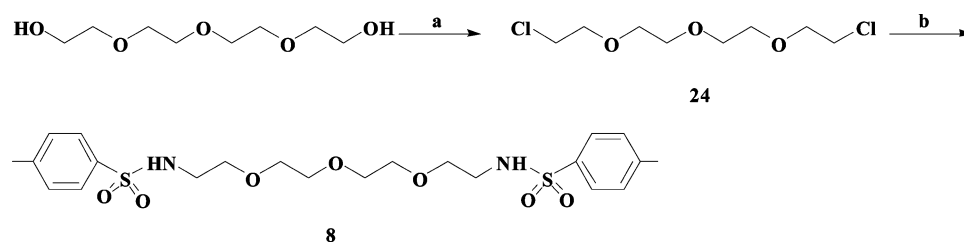
$$\Delta E_{\text{bind}} = E_{\text{complex}} - E_{\text{channel}} - E_{\text{mol}} \quad (1)$$

where E_{complex} , E_{channel} , and E_{mol} are respectively the total energies of the complexes, the K^+ channel, and the small molecules. The Tripos force field³² was used for structure optimization and energy calculation. At the same time, the $\log P$ values of these DOCK selected molecules were predicted using the XLOGP program.²⁷ The top 300 molecules produced from DOCK screening were analyzed for relatively lower binding energy, favorable shape complementarity, and/or potential in forming hydrogen bonds with K^+ channel and XlogP values. According to the DOCK scoring results, interaction models (shape complementarity and potential in hydrogen bond formation), and $\log P$ values, 20 compounds (**1–20**) were finally selected for biological assay, and their primary binding free energies with the K^+ channel were calculated using AutoDock 3.0.³⁴

2.1.3. Free Energy Calculation. The complex structures of the channel with the active compounds (inhibitors) were solvated by a TIP3P³⁵ water sphere with a radius of 25 Å. Then the solvent models were equilibrated for 600 ps at 300 K by using molecular dynamics (MD) simulation, and a 200 ps MD simulation was run on each model system to sample the conformations every 4 ps for binding free energy calculations. Only the solvent and those residues within 15 Å of the inhibitor were allowed to move during the MD simulation. All MD simulations were carried out by using the AMBER 7.0 program,³⁶ and the AMBER force field (parm98)³⁷ and general

Scheme 1. Chemical Structures of Compounds **5**, **6**, **8**, and **18–20**^a

^a Reagents: (a) PhONa, (b) NH₂OH·HCl; (c) LAH; (d) 10% hydrochloric acid.

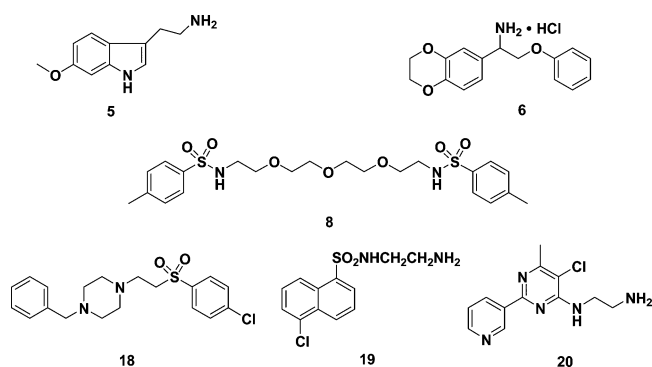
Scheme 2^a

^a Reagents: (a) SOCl₂, pyridine; (b) K₂CO₃, KI.

AMBER force field (GAFF)³⁸ were applied on the protein and the inhibitors, respectively. The partial charges for all the inhibitors were obtained by fitting the Hartree–Fock calculations with Gaussian 98 at the 6-31G* basis set level using RESP.³⁹ The MM/GBSA²⁸ method was used to evaluate the binding free energies (ΔG_{bind}) of the inhibitors to the K⁺ channel,

$$\begin{aligned}\Delta G_{\text{bind}} &= G_{\text{complex}} - G_{\text{protein}} - G_{\text{ligand}} \\ &= \Delta E_{\text{MM}} + \Delta G_{\text{GB}} + \Delta G_{\text{NP}}\end{aligned}\quad (2)$$

where ΔG_{GB} is the polar solvation energy in the continuum solvent, computed using a modified generalized Born model⁴⁰ and where the nonpolar contribution (ΔG_{NP}) was estimated using a simple empirical relation $\Delta G_{\text{NP}} = \sigma A + b$,⁴¹ where A is the solvent-accessible surface area estimated using the MSMS program,⁴² σ and b are empirical parameters, and in this work, 0.005 42 and 0.92 kcal/mol were adopted for these two parameters, respectively. ΔE_{MM} denotes the sum of the molecular mechanical (MM) energies of the molecules.



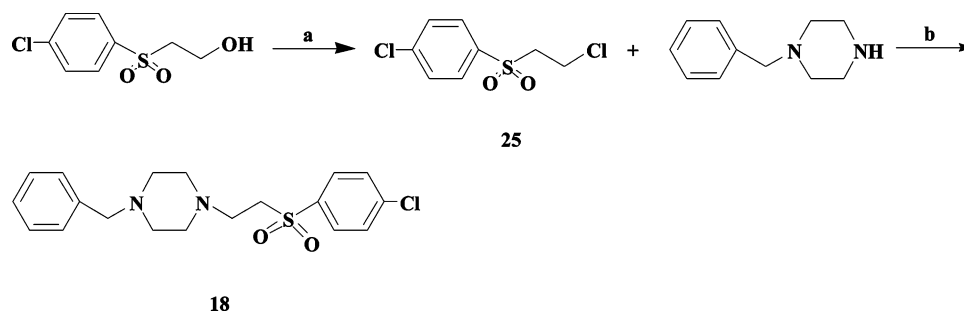
2.2. Compounds and Chemical Synthesis. On the basis of virtual screening, six compounds were selected as K⁺ channel inhibitor candidates for further electrophysiological assay. Compounds **5** and **20** were purchased from the Sigma and Maybridge companies, respectively. The spectral data of these

two compounds have been described in Table S1 in the Supporting Information. Compounds **6**, **8**, **18**, and **19** were synthesized by us. Scheme 1 depicts the sequence of reactions that led to the preparation of compound **6** by using 2-bromo-1-(2,3-dihydro-1,4-benzodioxin-6-yl)ethanone and sodium phenoxide as the starting raw materials. Intermediate 1-(2,3-dihydro-1,4-benzodioxin-6-yl)-2-phenoxyethanone (**21**) was synthesized by reacting the commercially available 2-bromo-1-(2,3-dihydro-1,4-benzodioxin-6-yl)ethanone with sodium phenoxide in THF. Then compound **21** was condensed with hydroxylamine hydrochloride by refluxing in ethanol, which afforded 1-(2,3-dihydro-1,4-benzodioxin-6-yl)-2-phenoxyethanone oxime (**22**). Compound **22** was reduced by LAH in THF, providing 1-(2,3-dihydro-1,4-benzodioxin-6-yl)-2-phenoxyethylamine (**23**). Compound **23** was changed into its hydrochloride, compound **6**, by the addition of 10% hydrochloric acid.

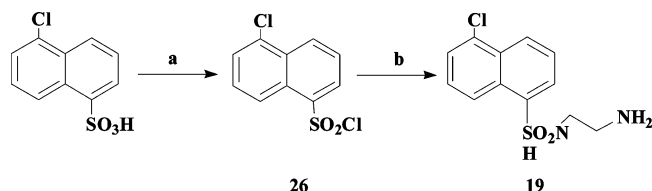
Scheme 2 depicts the sequence of reactions that led to the preparation of compound **8** by using tetraethylene glycol as the starting raw materials. Tetraethylene glycol was chlorinated using SOCl₂ in the presence of pyridine in 1,4-dioxane, providing bis[2-(2-chloroethoxy)ethyl] ether (**24**). Then compound **24** reacted with toluene-4-sulfonamide in DMF, using KI as a catalyst, which afforded the target compound **8**.

The starting raw materials for preparing compound **18** were commercially available 2-[(4-chlorophenyl)sulfonyl]ethanol and SOCl₂. Scheme 3 shows the procedures for preparation of the target compound. Intermediate 2-[(4-chlorophenyl)sulfonyl]ethanol was chlorinated by SOCl₂ in the presence of pyridine in toluene to yield 2-chloro-[(4-chlorophenyl)sulfonyl]ethane (**25**). Compound **25** reacted with 1-benzylpiperazine in THF, catalyzed by KI, providing the target molecule **18**.

Compound **19** was synthesized through the route outlined in Scheme 4, using 5-chloronaphthalene-1-sulfonic acid as the starting raw material. Intermediate 5-chloronaphthalene-1-sulfonic acid was chlorinated by PCl₅, providing 5-chloronaphthalene-1-sulfonyl chloride (**26**). Compound **26** reacted with 1,2-diaminoethane in the presence of K₂CO₃ in THF, giving the target compound **19**.

Scheme 3^a

^a Reagents: (a) SOCl₂, pyridine; (b) K₂CO₃, I₂.

Scheme 4^a

^a Reagents: (a) PCl₅; (b) H₂NCH₂CH₂NH₂.

2.3. Electrophysiological Assay. 2.3.1. Preparation of Dissociated Hippocampal Neurons. Dissociated CA1 pyramidal neurons were prepared from 5- to 9-day-old Sprague-Dawley rats as described previously.⁴³ Briefly, transverse minislices (500 μm) of the hippocampal CA1 region were cut in an oxygenated ice-cold dissociation solution. The dissociation solution consisted of the following (in mM): Na₂SO₄, 82; K₂SO₄, 30; MgCl₂, 5; *N*-(2-hydroxyethyl)piperazine-*N'*-(2-ethanesulfonic acid) (HEPES), 10; glucose, 10; at pH 7.3 with NaOH. The slices were incubated in the dissociation solution containing protease XXIII (3 mg/mL) at 32 °C for 8 min and then placed in the dissociation solution containing trypsin inhibitor type II-S (1 mg/mL) and bovine serum albumin (1 mg/mL) at room temperature under an oxygen atmosphere. Before recording, the slices were triturated using a series of fire-polished Pasteur pipettes with decreasing tip diameters. The neurons were placed in a recording dish and perfused with an external solution containing the following (in mM): NaCl, 135; KCl, 5; CaCl₂, 1; MgCl₂, 2; HEPES, 10; glucose, 10; tetrodotoxin, 0.001; at pH 7.3 with NaOH.

2.3.2. Whole-Cell Recording. Whole-cell voltage-clamp recording was made from pyramidal-shaped neurons using an Axopatch 200A amplifier (Axon Instruments) at 21–23 °C. The electrodes (tip resistance of 3–4 MΩ) were filled with a pipet solution containing the following (in mM): KCl, 140; MgCl₂, 1; CaCl₂, 1; HEPES, 10; EGTA, 10; at pH 7.3 with KOH. The neuron was held at –50 mV. Voltage-activated K⁺ currents were elicited with command protocols provided by pClamp 9.0 software via a DigiData-1322A interface (Axon Instruments). Signals were filtered at 2–10 kHz and sampled at frequencies of 10–40 kHz. Series resistance was compensated by 75–85%. Linear leak and residual capacitance currents were subtracted online. The peak amplitude of the fast transient K⁺ current (*I*_A) was measured. The amplitude of the delayed rectifier K⁺ current (*I*_K) was measured with 300 ms latency. For external application, the candidate compound was dissolved in the external solution, and delivered to the recorded neuron using RSC-100 rapid solution changer with a nine-tube head (BioLogic Co. France). For intracellular application, the compound was dissolved in the pipet solution and diffused from the pipet into the neuron after the patch membrane was ruptured.⁴⁴ The IC₅₀ values of

the six compounds were calculated using the computer software “GraphPad Prism 3.0”. Data are presented as mean ± SEM.

3. Results and Discussion

3.1. Identification of Compounds by Virtual Screening. Sequence alignment indicates that the identity between the pore regions of KcsA K⁺ channel and the Shaker K⁺ channels is 36.875% (Figure S1 in the Supporting Information). The optimized 3D model of the eukaryotic K⁺ channels is very similar to the X-ray crystal structure of KcsA K⁺ channel (Figure S2 in the Supporting Information). We can therefore use this 3D model for virtual screening. Virtual screening was performed on the ACD database²⁴ by using DOCK 4.0²⁵ targeting the 3D model of K⁺ channel. Before virtual screening, nondruglike structures were removed by a filter for druglike analysis²⁶ developed in our laboratory. Because compounds that plug the “ion-selective filter” of the K⁺ channel⁴⁵ may function as blockers of the channel, the extracellular pore binding site composed by the residues around the TXXTVGYG motif was used as the target site for virtual screening. The binding pose (orientation and conformation) of each molecule was evaluated by the DOCK scoring function, which consists of the van der Waals and Coulombic electrostatic interaction energies. The top-300 candidate molecules were selected from ACD for further analysis (Figure 2A, Figure S3). The DOCK scoring indicates that electrostatic interaction dominates the binding between the candidates and K⁺ channel. This is in agreement with the free energy calculation for the active compounds with the K⁺ channel (see discussion below).

However, docking programs and scoring functions have a tendency to generate a significant number of false positives.¹⁷ Accordingly, the structures of the complexes of the top-300 molecules with the K⁺ channel were optimized in the Sybyl6.7³² environment by running a SPL³² program written by us to adjust the binding pose, and the binding energies (ΔE_{bind}) were recalculated by using a more sophisticated method, molecular mechanics force field (see eq 1 in Materials and Methods). The interaction energies of these 300 molecules with the K⁺ channel calculated by DOCK range from –38.33 to –22.76 kcal/mol and that calculated by Sybyl are from –178.85 to –72.15 kcal/mol (Figure 2B). More than 50% candidate molecules are located in the high interaction energy area on the DOCK-Sybyl plot (top-right part of Figure 2B). These molecules would not be considered for further analysis. Most of the rest of the candidate molecules are dispersed at the top-left part of the plot (red rectangle), and several molecules are displayed in the lower-middle region of the plot (green rectangle). There are almost no points at the bottom-left. It is therefore difficult to select candidates directly from the red and green rectangles, and other factors have to be considered in compound selection.

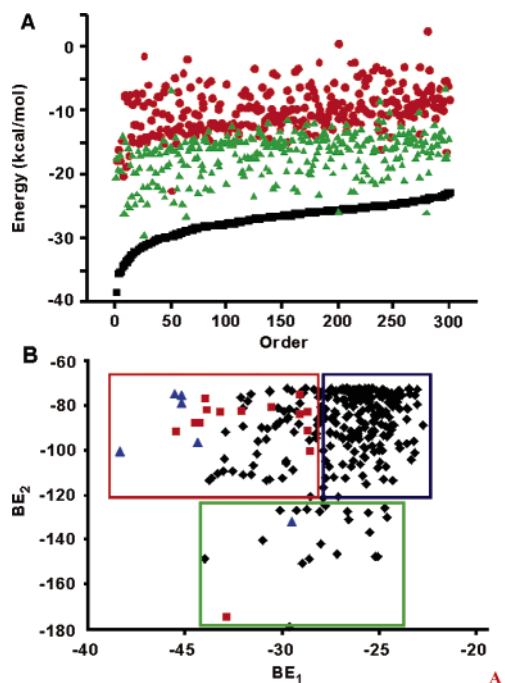


Figure 2. Binding energies of the top-300 compounds: (A) DOCK binding energies (black ■, total binding energy; red ●, van de Waals energy; green ▲, electrostatic energy); (B) DOCK predicted binding energies (BE_1) versus Sybyl binding energies (BE_2) (blue ▲, compounds 5–6, 8, 18–20; red ■, compounds 1–4, 7, 9–17; black ◆, compounds 21–300).

Hydrophobicity is an important druglike property of molecules. As described in our previous study,²³ the MDL Drug Data Report (MDDR) database⁴⁶ contains 206 potent K^+ channel inhibitors, and 10 of them have entered into clinical trial. We have calculated the $\log P$ values for these K^+ channel inhibitors by use of the XLOG program.²⁷ The result indicated that 70% of the K^+ channel inhibitors in MDDR show $\log P$ values from 0 to 6, and nine of the clinical inhibitors showed $\log P$ values from 2 to 6.²³ Accordingly, candidate molecules should have similar $\log P$ values compared with existing K^+ channel inhibitors. Synthetically considering the two kinds of interaction energies and the $\log P$ values (is better between 0 and 6) and a visual check of the interaction models, 20 molecules were selected for bioassay, 18 from the red rectangle and 2 from the green one (Figure 2B). The predicted $\log P$ values of most of the 20 selected candidates are within or close to 0–6. Only 4 compounds (2, 7, 10, and 16) are outside the region of the $\log P$ profile of the existing K^+ channel inhibitors (Table 1). As will be seen below, these four compounds are inactive, suggesting the importance of hydrophobicity in the selection of K^+ channel inhibitors.

3.2. Compounds Synthesis. The 20 candidate compounds were purchased from the Sigma and Maybridge companies for the primary screening. Among the six active compounds, only enough chemical samples of compounds 5 and 20 could be supported respectively by the Sigma and Maybridge companies for further bioassay. The spectral data of these two compounds have been described in Table S1 in the Supporting Information. Because the companies could not provide enough samples for compounds 6, 8, 18, and 19, they were synthesized through the routes outlined in Schemes 1–4, and the details of the synthetic procedures and structural characterizations are described in the Experimental Section. The purities of these six compounds are listed in Table S2 in the Supporting Information.

Table 1. Binding Energies (in kcal/mol), Actual Ranks, and XlogP Values of the 20 Compounds Selected from the 300 Candidates^a

compd	BE_1^b	R_1^b	BE_2^c	R_2^c	BE_3^d	R_3^d	XlogP
1	-33.85	9	-82.245	167	-16.57	14	0.35
2	-29.10	57	-84.331	154	-45.68	3	-2.09
3	-32.82	13	-175.019	2	-26.52	7	4.42
4	-35.40	3	-92.112	104	-45.95	2	0.51
5	-35.16	4	-75.437	225	-16.33	16	1.29
6	-34.32	7	-96.668	80	-15.23	17	2.59
7	-28.67	64	-91.259	110	6.64	22	-0.89
8	-29.51	51	-132.34	12	-9.81	20	1.87
9	-29.06	57	-75.32	227	-6.14	21	5.05
10	-30.49	33	-81.235	176	-46.50	1	-1.13
11	-32.96	11	-103.654	59	-27.32	6	0.15
12	-33.12	10	-83.070	161	-13.74	18	0.96
13	-28.67	64	-83.269	160	-22.71	11	-0.12
14	-32.21	15	-87.947	131	-42.21	4	-0.19
15	-33.90	9	-77.120	205	-16.34	15	-0.49
16	-34.46	6	-87.807	132	-11.31	19	-1.82
17	-28.51	68	-100.82	64	-25.57	10	0.19
18	-35.50	2	-75.069	231	-25.57	9	3.31
19	-38.33	1	-100.505	67	-17.00	13	2.00
20	-35.16	4	-78.822	191	-17.29	12	1.04

^a Boldfaced and italic values are for the six active compounds discussed in the text. ^b The binding energy (BE_1) and the actual rank (R_1) calculated using DOCK. ^c The binding energy (BE_2) and the actual rank (R_2) calculated using Sybyl. ^d The binding energy (BE_3) and the actual rank (R_3) calculated using AutoDock.

3.3. K^+ Channel-Blocking Effects of Candidate Compounds.

3.3.1. Primary Electrophysiological Assay. In the primary electrophysiological assay, 20 candidate compounds selected from the virtual screening were determined using the whole-cell voltage-clamp recording from dissociated hippocampal neurons. When applied externally, six candidate compounds (5, 6, 8, 18, 19, and 20) at 100 μ M suppressed at least one type of the K^+ current (I_K or I_A) by more than 10%, whereas the other 14 compounds at 100 μ M and even at 1 mM had no significant effect. Each of the six compounds more markedly suppressed I_K than I_A . The results are shown in Figure 3A and Table S3 in the Supporting Information.

3.3.2. Secondary Electrophysiological Assay. The secondary electrophysiological assay was conducted to determine the concentration–response relationship for the six candidate compounds. The result is shown in Figure 3B. The IC_{50} values of these compounds obtained via curve-fitting procedures are presented in Table 2. All six compounds potently blocked both types of K^+ currents with IC_{50} values ranging from a few μ M to nearly 1 mM. The rank order of potency in inhibition of I_K (8 > 19 > 18 > 6 > 20 > 5) was basically parallel to that of inhibition of I_A (8 > 19 > 20 > 6 > 5 > 18). The ratio of IC_{50} values in inhibition of I_A to those of I_K represented the selectivity of a compound for two types of K^+ channels. For the six compounds, the ratio of IC_{50} values ranged from 1.9 to 16.3. Compound 18 shows the highest selectivity for I_K ($IC_{50}(I_K)/IC_{50}(I_A) = 16.3$), whereas compound 5 is the least selective ($IC_{50}(I_K)/IC_{50}(I_A) = 1.9$).

3.3.3. Intracellular Application of the Candidate Compounds. Externally applied chemicals, like verapamil, could diffuse through the membrane and block the K^+ channels at an internal binding site.⁴⁹ In order to exclude the possibility, the effects of intracellular application of the six compounds on the K^+ currents were investigated. Each compound was included in the recording pipet at a concentration that could inhibit I_K by more than 75% when applied externally and diffused into the neuron after the membrane ruptured.⁴⁴ As shown in Figure 4, all six compounds had no detectable effect on I_K nor did the compounds affect I_A (data not shown). The results suggest that

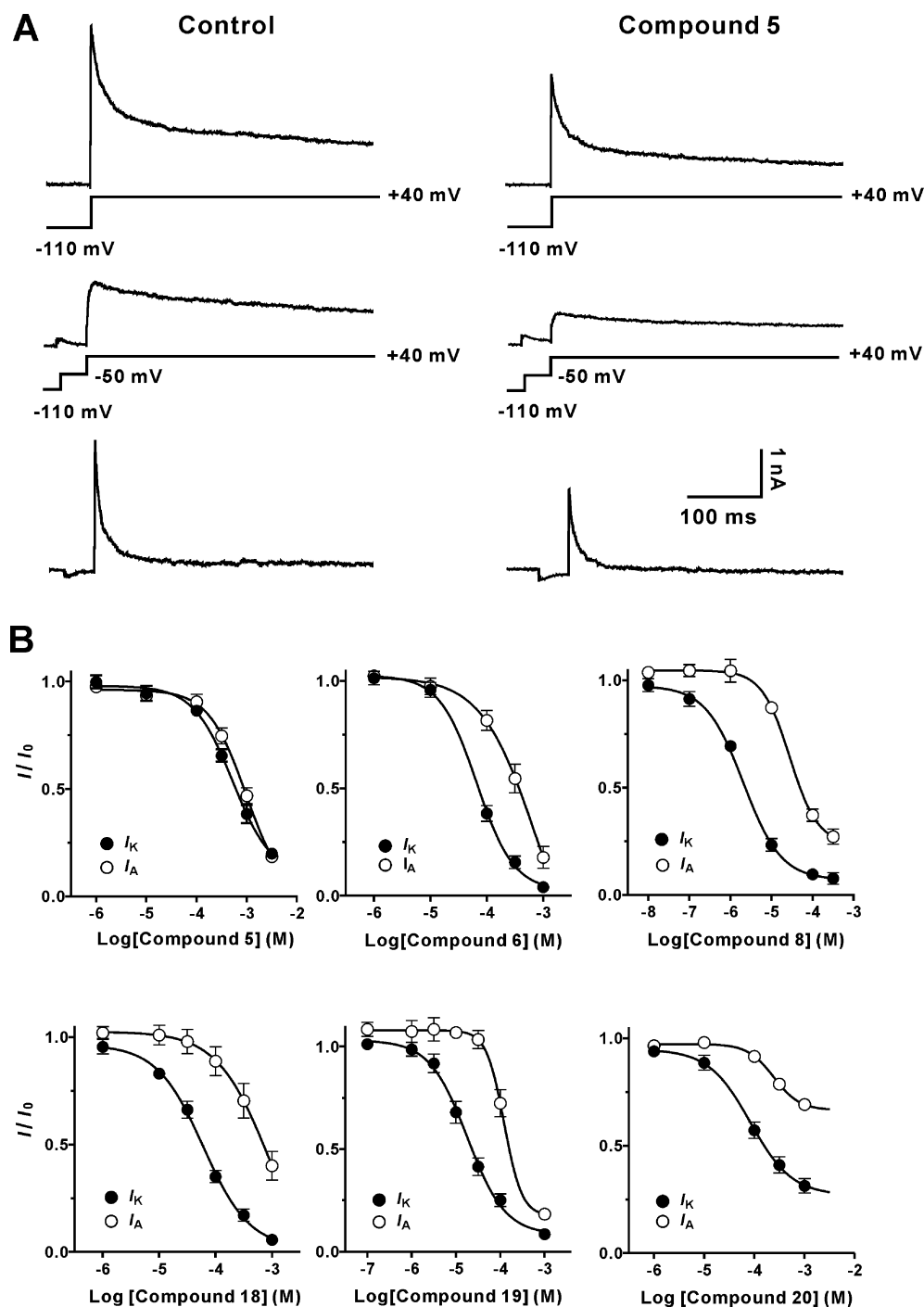


Figure 3. Effects of the externally applied six compounds on voltage-activated K⁺ currents in rat hippocampal neurons. (A) The total K⁺ current (upper record), delayed rectifying K⁺ current (*I*_K, middle record), and fast transient K⁺ current (*I*_A, lower record) were recorded in control and in the presence of compound **5** (500 μM). The traces at the bottom of the upper and middle records are the command voltage steps. The neuron was held at -50 mV. The total K⁺ current was elicited by a depolarizing step to +40 mV following a hyperpolarizing prepulse of 500 ms to -110 mV. *I*_K was elicited by a similar protocol in which a 50 ms interval at -50 mV was inserted after the prepulse. *I*_A was the subtraction of *I*_K from the total K⁺ current.^{43,47–48} (B) Concentration–response curves of the six compounds in inhibition of *I*_K and *I*_A. Each symbol represents the mean ± SEM (*n* = 5–12).

the six compounds bind to an external site of the K⁺ channels, thus blocking the K⁺ currents.

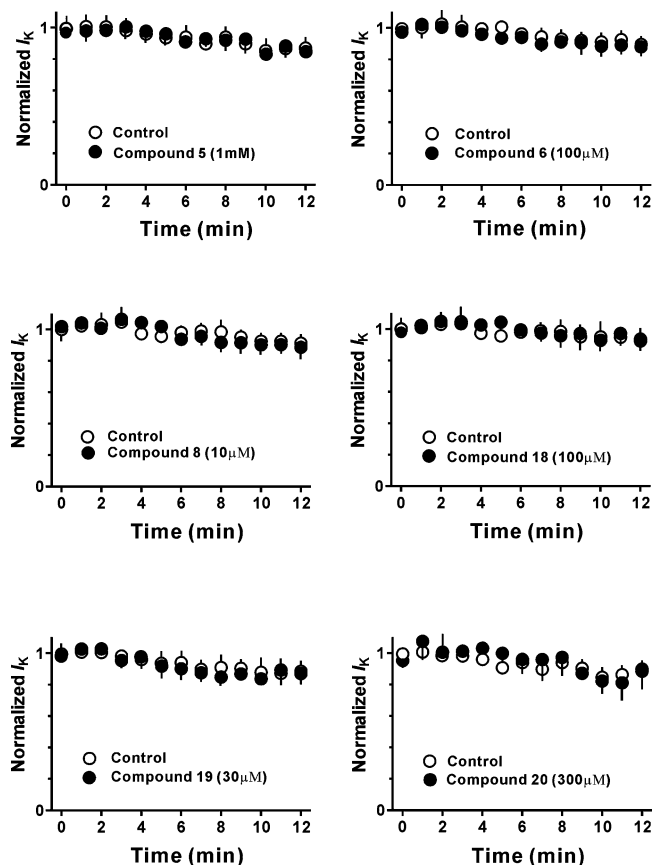
3.4. Structure–Activity Relationship (SAR). If we reappraise the virtual screening result with the active compounds, it can be seen that five active compounds are in the lowest DOCK interaction energy region and one is in the low Sybyl interaction energy region (Figure 2B). As mentioned above, most of the clinical K⁺ channel inhibitors showed log *P* values from 2 to 6.²³ The log *P* values of the six active compounds range from 1.0 to 3.5 (Table 1), indicating that the discovered active

compounds possess good hydrophobic profiles similar to those of the existing K⁺ inhibitors. This may be one of the reasons why only these 6 compounds are active among the 20 candidates.

The general interaction models of the six compounds with the K⁺ channel are presented in Table S4 in the Supporting Information and Figure 5. The binding free energies of the six compounds to the K⁺ channel were calculated by the MM/GBSA²⁸ method encoded in the AMBER program, version 7.0,³⁶ and the results are listed in Table 3. The result indicates that

Table 2. IC₅₀ Values of the Six Compounds in Inhibition of the Voltage-Activated K⁺ Currents

compd	IC ₅₀ (μM)		IC ₅₀ (I _A)/IC ₅₀ (I _K)	n ^a
	I _K	I _A		
5	524 ± 14	972 ± 34	1.9	6
6	67 ± 9	737 ± 48	11	6
8	2.1 ± 0.5	28 ± 4	13.3	6
18	60 ± 7	980 ± 150	16.3	6
19	18 ± 3	124 ± 9	6.9	6
20	83 ± 8	244 ± 26	2.9	6

^a n: the number of neurons tested.**Figure 4.** Time course of the delayed rectifier K⁺ current (I_K) in rat hippocampal neurons during intracellular application of the six compounds. In each panel, the normalized I_K is plotted against the time of intracellular application of the compounds. Each symbol represents the mean ± SEM (n = 5). The concentrations chosen for intracellular application were above the IC₇₅ values (causing 75% inhibition of I_K) of the same compounds in external application: compound 5 (1 mM), compound 6 (100 μM), compound 8 (10 μM), compound 18 (100 μM), compound 19 (30 μM), and compound 20 (300 μM).

the calculated MM/GBSA binding free energies correlate well with the inhibitory activities ($R = 0.83$), as shown in Figure 6A. This relationship suggests that those potential K⁺ channel inhibitors exhibiting stronger binding free energies using this paradigm would therefore expect to have greater efficacy toward inhibitory action. The results demonstrated the efficiency of our strategy for discovering potassium channel blockers by using virtual screening in conjunction with electrophysiological assay.

Structurally, compounds 5, 6, and 18–20 have similar chemical scaffolds with amino groups that are easily protonated to be quaternary ammoniums in vivo. The amino group of compounds 5, 6, 19, and 20 acts as a donor to form hydrogen bonds with the O atoms of Gly77(A–D) and Tyr78(A–D) of the K⁺ channel, respectively (Figure 5 and Table S4 in the Supporting Information). These hydrogen bonds play vital roles

for these compounds binding to the K⁺ channel, and this may be an important reason that these compounds could potentially inhibit K⁺ channel. Compounds 5, 6, 8, and 18–20 bind with the side chains of residues Ser57(A), Tyr78(B–D), Gly79(A, B, D), Asp80(B, D), Thr82(C, D), and Val84(A) of the K⁺ channel through both hydrophobic interactions and electrostatic interactions (Figure 5 and Table S4 of the Supporting Information). The number of hydrophobic contact pairs is not consistent with inhibitory potency, indicating that the difference in inhibitory activities of these compounds might be contribution of complex effects related to hydrogen bonding, hydrophobic contact, electrostatic interaction, and solvation. The correlation between the van der Waals binding energies and log IC₅₀ values ($R = 0.75$, Figure 6B) indicates that the van der Waals interaction demonstrates structure–activity relationship (SAR) of the six compounds. Although the electrostatic binding energy for each compound to the K⁺ channel is the determinant component in the molecular mechanical energy (Figure 2A and Table 3), the polar solvation energy penalty is also high, which counteracts the electrostatic interaction.

Among the six compounds, compound 8 shows the most potent inhibitory activity (Table 2). In line with the bioassay result, MM/GBSA calculations indicated that compound 8 binds to the K⁺ channel with the lowest binding free energy (Table 3). The components of the binding free energy of this compound are also different from those of other compounds (Table 3). The electrostatic interaction of compound 8 with the K⁺ channel is much weaker than that of other compounds. This is also in agreement with the interaction models (Figure 5), indicating that only compound 8 did not form a hydrogen bond to the K⁺ channel. However, the solvation free energy (G_{b,sur} + G_b) of compound 8 is remarkably smaller than that of other compounds (Table 3), suggesting that this compound can easily overcome the bondage of solvent during binding to the K⁺ channel. In addition, the hydrophobic interaction of compound 8 to the K⁺ channel reflected by the van der Waals binding energy is also the strongest among the six compounds. Consequently, comprehensive effects of the electrostatic interaction, hydrophobic interaction, and solvation make compound 8 the most potent inhibitor of the K⁺ channel among the six compounds.

4. Conclusions

As mentioned above, high-throughput screening (HTS) has not been applied to discover K⁺ channel blockers because of the hindrance of the electrophysiological assay. Previously, we discovered four natural K⁺ channel blockers by using docking based virtual screening in conjunction with an electrophysiological assay.²³ Here, we further demonstrated the effectiveness of the strategy for discovering K⁺ channel blockers from the synthetic chemicals. The molecular docking program DOCK4.0²⁵ was used to screen the chemical database ACD²⁴ targeting the 3D model of the Shaker K⁺ channel. The top-300 molecules were obtained by the scoring function of DOCK. Then the complexes of these 300 candidates with the K⁺ channel model were optimized by molecular mechanics encoded in Sybyl and the interaction energies were calculated. In addition, the log *P* values of these molecules were predicted by the XlogP program.²⁷ According to the interaction energies, the DOCK scoring result, and the XlogP values, 20 compounds were selected and re-estimated using AutoDock.³⁴ The bioassay results demonstrated a relatively high hit rate of our virtual screening approach. Of the 20 candidates, 6 compounds (5, 6, 8, 18–20) were found to suppress at least one type of voltage-activated K⁺ current (I_K or I_A) by more than 10%. Furthermore,

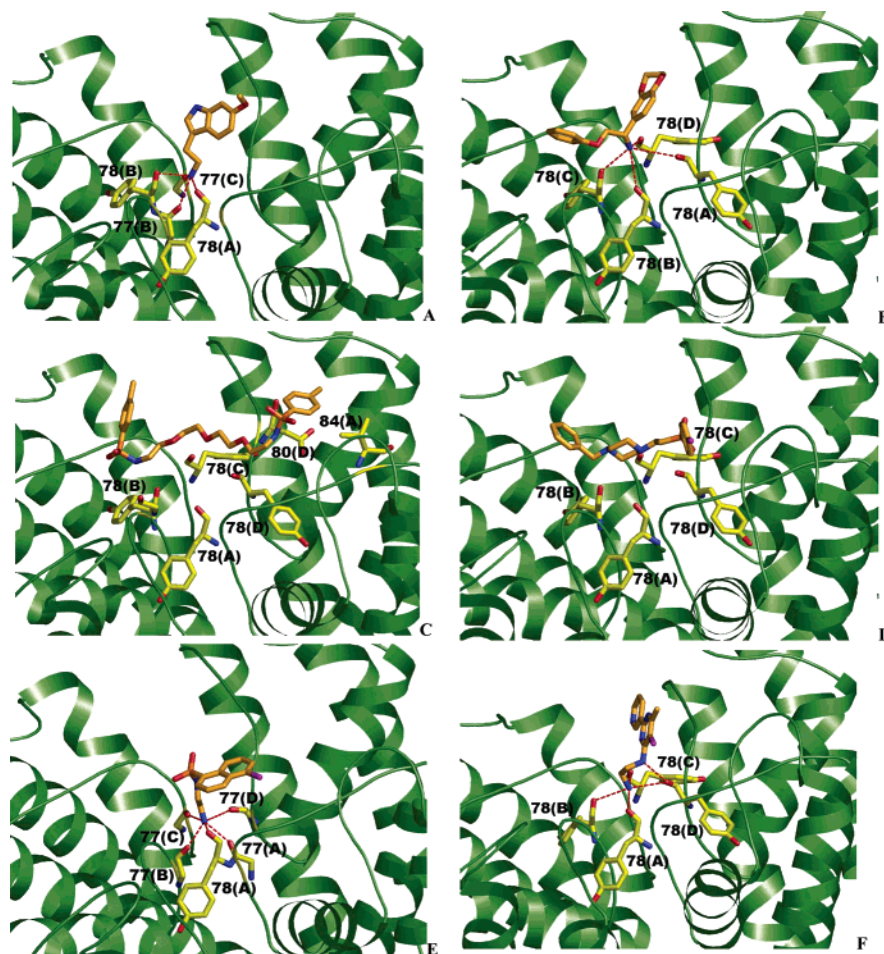


Figure 5. 3D representatives for the general interaction models of compounds **5** (A), **6** (B), **8** (C), **18** (D), **19** (E), and **20** (F) with the potassium ion channel. The broken lines in red represent hydrogen bonds. This picture was produced by using the PyMOL program.⁵⁰

Table 3. Binding Free Energies of the Six Compounds to the K⁺ Channel (kcal/mol)

compd	log IC ₅₀	<i>E</i> _{ele} ^a	<i>E</i> _{vdw} ^b	<i>E</i> _{MM} ^c	G _{sur} ^d	G _b ^e	G _{sol} ^f	G _{bind} ^g
5	-3.28	-220.06	-27.10	-247.15	-2.37	245.73	243.36	-3.80 ± 2.60
6	-4.17	-219.27	-23.14	-242.42	-2.26	227.70	225.44	-16.98 ± 2.53
8	-5.68	-42.22	-42.16	-84.38	-3.02	67.43	64.41	-19.97 ± 2.54
18	-4.22	-330.40	-30.14	-360.53	-2.79	352.21	349.42	-11.11 ± 3.77
19	-4.74	-234.63	-33.10	-267.73	-2.77	257.64	254.86	-12.86 ± 2.89
20	-4.08	-256.31	-18.01	-274.32	-2.05	269.12	267.07	-7.25 ± 2.83

^a Nonbonded electrostatic energy. ^b Nonbonded van der Waals energy. ^c The molecular mechanical energy ($=E_{\text{ele}} + E_{\text{vdw}}$). ^d Hydrophobic contribution to the solvation free energy, which is determined with solvent accessible surface area terms. ^e Electrostatic contribution to the solvation free energy, which is calculated with the generalized Born method. ^f The solvation free energy ($=G_{\text{sur}} + G_{\text{b}}$). ^g The binding free energy ($=G_{\text{sol}} + E_{\text{MM}}$).

the 6 compounds preferentially blocked *I_K* rather than *I_A* with a ratio of IC₅₀(*I_A*)/IC₅₀(*I_K*) ranging from 1.9 to 16.3 (Figure 3 and Table 2). In addition, the interaction features of these compounds with the K⁺ channel were mapped (Figure 5 and Table S4 in the Supporting Information) and provide clear clues for further structural modification for the six compounds. The calculated binding free energies of the six compounds to the K⁺ channel are in agreement with their inhibitory potency (Figure 6). The hydrogen bonding and solvation penalty play important roles for the binding affinity between the compounds and the channel. The strategy used in this paper provides a mode for quickly discovering new K⁺ channel blockers from large databases, especially when the HTS of K⁺ channel is current not available.

5. Experimental Section

The reagents (chemicals) were purchased from Shanghai Chemical Reagent Company and were used without further purification.

Yields were not optimized. Melting points were measured in a capillary tube and were uncorrected. Infrared (IR) spectra were determined using a Bruker IFS-48 FT-IR spectrometer. Solids were prepared with potassium bromide (KBr) disks, and the results were reported in wavenumbers (cm⁻¹). Nuclear magnetic resonance (NMR) spectra were determined using a Bruker AMX-400 spectrometer referenced to Me₄Si. Chemical shifts are reported in parts per million (ppm, downfield from tetramethylsilane). Splitting patterns are described as singlet (s), doublet (d), triplet (t), quartet (q), multiplet (m), and broad (br). Low- and high-resolution mass spectra (LRMS and HRMS) were obtained by electric or chemical ionization (ESI) produced by a MAT-95 spectrometer.

1-(2,3-Dihydro-1,4-benzodioxin-6-yl)-2-phenoxyethylamine Hydrochloride (6). A solution of phenol sodium salt (1.74 g, 0.015 mol) in THF (20 mL) was added dropwise to a solution of 2-bromo-1-(2,3-dihydro-1,4-benzodioxin-6-yl)ethanone (2.57 g, 0.01 mol) in THF (15 mL) and continually refluxed for 3 h with constant stirring. Thereafter, water (20 mL) was added and stirred at room temperature for 15 min and then extracted with dichloromethane

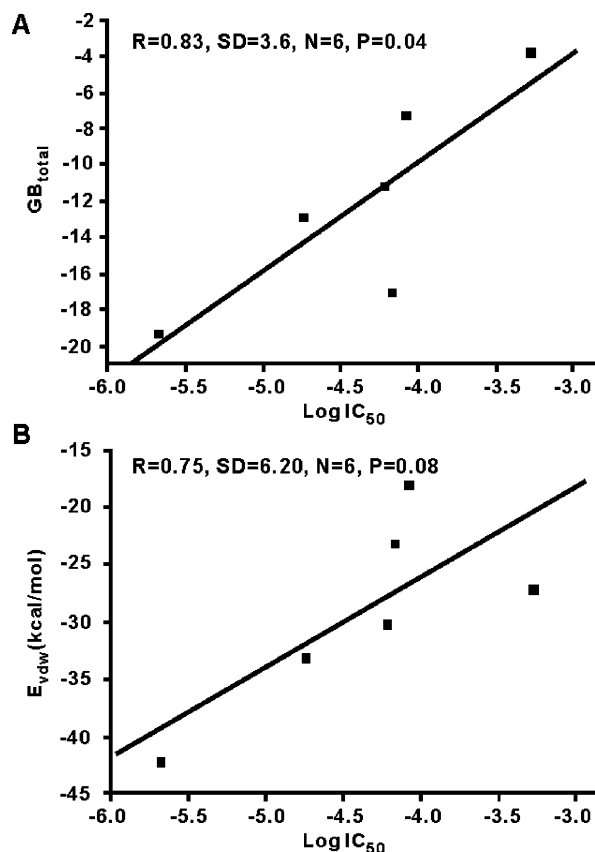


Figure 6. (A) Correlation between the calculated binding free energies (GB_{total} , kcal/mol, $T = 300$ K) of the six compounds and the experimental activities ($\log IC_{50}$). (B) Correlation between van de Waals energies (E_{vdw} , kcal/mol, $T = 300$ K) of the six compounds and the experimental activities ($\log IC_{50}$).

(3 × 20 mL). The final organic layer was dried over anhydrous Na_2SO_4 , and the solvent was removed by evaporation under vacuum. After flash chromatography with dichloromethane–petroleum (2:1; v/v), 1-(2,3-dihydro-1,4-benzodioxin-6-yl)-2-phenoxyethanone (**21**) was obtained as a white semisolid (1.86 g), yield 68.6%.

A mixture of **21** (1.35 g, 5 mmol) and hydroxylamine hydrochloride (0.70 g, 10 mmol) in ethanol (20 mL) was refluxed for 2 h with constant stirring and then condensed. The crude 1-(2,3-dihydro-1,4-benzodioxin-6-yl)-2-phenoxyethanone oxime (**22**) was obtained as a pale semisolid (1.81 g), yield 88.5%.

To the solution of the crude **22** (1.0 g, 3 mmol) in THF (10 mL), $LiAlH_4$ (0.56 g 15 mmol) was added in portions. Thereafter, the mixture was stirred for 3 h, then ice–water (10 mL) was added and extracted with dichloromethane (3 × 20 mL). The final organic layer was dried under anhydrous Na_2SO_4 and condensed. After flash chromatography with ethyl acetate–petroleum (1:4; v/v), 1-(2,3-dihydro-1,4-benzodioxin-6-yl)-2-phenoxyethylamine (**23**) was obtained as a pale oil (0.52 g), yield 40.6%. A solution of 10% hydrochloric acid (2 mL) was added dropwise to a cold solution (0–5 °C) of **23** (0.256 g, 1 mmol) in dichloromethane (5 mL). After stirring for 15 min, the salt was filtered and recrystallized in 10% hydrochloric acid. Compound **6** was obtained as a pale solid, 0.24 g (82.1%), mp 236–238 °C. IR (KBr): 3425, 1589, 1498 cm^{-1} . 1H NMR ($CDCl_3$): δ 3.98 (t, 1H), 4.05 (q, 2H), 6.92 (m, 6H), 7.27 (m, 2H). HRMS (SCI) m/z calcd for M^+ , 271.1208; found, 271.1198. Anal. ($C_{16}H_{17}NO_3 \cdot HCl$). Calcd, C 62.44, H 5.89, N 4.55; found, C 62.40, H 5.61, N 4.52.

1,11-Di{[(4-methylphenyl)sulfonyl]amino}-3,6,9-trioxaundecane (8). A solution of $SOCl_2$ (0.708 g, 6.0 mmol) in 1,4-dioxane (5 mL) was added slowly to a cold solution (0–5 °C) of tetraethylene glycol (1.94 g, 10 mmol) and pyridine (1 mL) in 1,4-

dioxane (25 mL) and then refluxed for 3 h, quenched with ice–water (120 mL), and extracted with dichloromethane (3 × 20 mL). The organic layer was dried over anhydrous Na_2SO_4 and condensed. After flash chromatography with ethyl acetate–petroleum (1:10; v/v), bis[2-(2-chloroethoxy)ethyl] ether (**24**) was obtained as yellowish oil (1.27 g), yield 55.0%.

A mixture of **24** (0.231 g, 1.0 mmol), toluene-4-sulfonamide (0.428 g, 2.5 mmol), K_2CO_3 (0.345 g, 2.5 mmol), and KI (0.023 g) in DMF (3 mL) was stirred for 24 h at 100 °C, then quenched with ice–water, extracted with dichloromethane (3 × 10 mL), dried under anhydrous Na_2SO_4 , and condensed. After flash chromatography with ethyl acetate–petroleum (1:3; v/v), compound **8** was obtained as a white solid (0.388 g), yield 77.6%. IR (KBr): 1596, 1480 cm^{-1} . 1H NMR ($CDCl_3$): δ 2.30 (s, 2H), 2.38 (s, 6H), 3.48 (t, 4H), 3.53 (t, 12H), 7.25 (m, 4H), 7.72 (m, 4H). HRMS (SCI) m/z calcd for M^+ , 500.1651; found, 500.1682. Anal. ($C_{22}H_{32}N_2S_2O_7$). Calcd, C 52.78, H 6.44, N 5.60; found, C 52.80, H 6.43, N 5.58.

1-Benzyl-4-[2-[(4-chlorophenyl)sulfonyl]ethyl]piperazine (18). The solution of $SOCl_2$ (0.354 g, 3.0 mmol) in toluene (10 mL) was added dropwise to a solution of 2-[(4-chlorophenyl)sulfonyl]ethanol (0.220 g, 1.0 mmol) and 10 drops of pyridine in toluene (15 mL) in an ice–water bath. Then the mixture was refluxed for 3 h, then ice–water (10 mL) was added, and it was extracted with dichloromethane (3 × 10 mL), dried under anhydrous Na_2SO_4 , and condensed. After flash chromatography with ethyl acetate–petroleum (1:20; v/v), 2-chloro[4-(4-chlorophenyl)sulfonyl]ethane (**25**) was obtained as a pale oil, 0.21 g, yield 87.5%.

A mixture of **25** (0.238 g, 1 mmol), 1-benzylpiperazine (0.176 g, 1 mmol), K_2CO_3 (0.207 g, 1.5 mmol), and I_2 (0.02 g) in THF (20 mL) was refluxed for 3 h with constant stirring and condensed. Then water (20 mL) was added and extracted with dichloromethane (3 × 15 mL). The final organic layer was dried under anhydrous Na_2SO_4 . After flash chromatography with ethyl acetate–petroleum (1:6; v/v), 1-benzyl-4-[2-[(4-chlorophenyl)sulfonyl]ethyl]piperazine (**18**) was obtained as a pale semisolid, 0.312 g, yield 82.3%. IR (KBr): 3448, 1579, 1479 cm^{-1} . 1H NMR ($CDCl_3$): δ 2.62 (t, 8H), 2.55 (t, 4H), 3.75 (t, 4H), 3.84 (s, 2H), 7.25 (m, 5H), 7.50 (m, 2H), 7.83 (m, 2H). HRMS (SCI) m/z calcd for M^+ , 378.1169; found, 378.1182. Anal. ($C_{19}H_{23}ClN_2O_2S$). Calcd, C 60.23, H 6.12, N 7.39; found, C 60.23, H 6.15, N 7.39.

N-(2-Aminoethyl)-5-chloronaphthalene-1-sulfonamide (19). The powder of 5-chloronaphthalene-1-sulfonic acid (2.42 g, 10 mmol) and PCl_5 (12.1 g) was mixed and heated to 80–90 °C and stirred for 1 h. Then the mixture was stirred at room temperature overnight. After flash chromatography with ethyl acetate–petroleum (1:8; v/v), 5-chloronaphthalene-1-sulfonyl chloride (**26**) was gained as a yellowish oil, 1.6 g, yield 61.5%.

A solution of 1,2-diaminoethane (0.072 g, 1.2 mmol) in THF (30 mL) was added dropwise to a mixture of **26** (0.26 g, 1 mmol), 30 mL of THF, K_2CO_3 (1.3 g) in an ice–water bath, then stirred at room temperature for 1 h and condensed. After flash chromatography with dichloromethane–ethanol (10:1; v/v), **19** was obtained as a yellow oil (178.4 mg), yield 82.2%. IR (KBr): 1605 cm^{-1} . 1H NMR ($CDCl_3$): δ 1.60 (s, 2H), 2.35 (t, 2H), 6.85 (s, 1H), 7.50 (d, 2H), 8.35 (d, 2H), 8.45 (m, 2H). HRMS (SCI) m/z calcd for M^+ , 284.0386; found, 284.0373. Anal. ($C_{12}H_{13}ClN_2SO_2$). Calcd, C 44.87, H 4.39, N 8.72; found, C 44.76, H 4.71, N 8.44.

Acknowledgment. The authors thank Professor I. D. Kuntz and Professor Arthur J. Olson for their kindness in offering the DOCK 4.0 and AutoDock 3.0.3 programs. We gratefully acknowledge financial support from the State Key Program of Basic Research of China (Grant 2002CB512802), the National Natural Science Foundation of China (Grants 29725203, 20472094, and 30472086), the Basic Research Project for Talent Research Group from the Science and Technology Commission of Shanghai, the Key Project from the Science and Technology Commission of Shanghai (Grants 02DJ14006 and 03ZR14110), and the Key Project for New Drug Research from CAS.

Supporting Information Available: Figures S1–S3 showing the sequence alignment of the KcsA and Shaker K⁺ channel pore regions, the structure superposition of the 3D model of eukaryotic Shaker K⁺ channel with the X-ray crystal structure of KcsA K⁺ channel, and the log *P* value distributions of the K⁺ channel inhibitors in the top-300 compounds picked from the ACD database; Tables S1–S4 listing the IR, ¹H NMR, and MS spectral data, element analysis results, HPLC analysis results, the effects of the selected 20 compounds on the voltage-dependent K⁺ currents in rat hippocampal neurons, and the hydrogen-bonding pairs and the hydrophobic contacts of compounds **5**, **6**, **8**, **18–20** with the K⁺ channel derived from AutoDock simulations. This material is available free of charge via the Internet at <http://pubs.acs.org>.

References

- Coetzee, W. A.; Amarillo, Y.; Chiu, J.; Chow, A.; Lau, D.; McCormack, T.; Moreno, H.; Nadal, M. S.; Ozaita, A.; Pountney, D. Molecular diversity of K⁺ channels. *Ann. N.Y. Acad. Sci.* **1999**, *868*, 233–285.
- Garcia, M. L.; Hanner, M.; Knaus, H. G.; Koch, R.; Schmalhofer, W.; Slaughter, R. S.; Kaczorowski, G. J. Pharmacology of potassium channels. *Adv. Pharmacol.* **1997**, *39*, 425–471.
- Kaczorowski, G. J.; Garcia, M. Pharmacology of voltage-gated and calcium-activated potassium channels. *Curr. Opin. Chem. Biol.* **1999**, *3*, 448–458.
- Coetzee, W. A.; Amarillo, Y.; Chiu, J.; Chow, A.; Lau, D.; McCormack, T.; Moreno, H.; Nadal, M. S.; Ozaita, A.; Pountney, D.; Saganich, M.; Vega-Saenz De Miera, E.; Rudy, B. Molecular diversity of K⁺ channels. *Ann. N.Y. Acad. Sci.* **1999**, *868*, 233–285.
- Wickenden, A. D. K⁺ channels as therapeutic drug targets. *Pharmacol. Ther.* **2002**, *94*, 157–182.
- Ashcroft, F. M. From molecule to malady. *Nature* **2006**, *440*, 440–447.
- Doyle, D. A.; Cabral, J. M.; Pfuetzner, R. A.; Kuo, A.; Gulbis, J. M.; Cohen, S. L.; Chait, B. T.; MacKinnon, R. The structure of the potassium channel: molecular basis of K⁺ conduction and selectivity. *Science* **1998**, *280*, 69–77.
- Zhou, Y. F.; Morais-Cabral, J. H.; Kaufman, A.; MacKinnon, R. Chemistry of ion coordination and hydration revealed by a K⁺ channel–Fab complex at 2.0 Å resolution. *Nature* **2001**, *414*, 43–48.
- Jiang, Y.; Lee, A.; Chen, J.; Cadene, M.; Chait, B. T.; MacKinnon, R. Crystal structure and mechanism of a calcium-gated potassium channel. *Nature* **2002**, *417*, 515–522.
- Jiang, Y.; Lee, A.; Chen, J.; Ruta, V.; Cadene, M.; Chait, B. T.; MacKinnon, R. X-ray structure of a voltage-dependent K⁺ channel. *Nature* **2003**, *423*, 33–41.
- Long, S. B.; Campbell, E. B.; MacKinnon, R. Crystal structure of a mammalian voltage-dependent Shaker family K⁺ channel. *Science* **2005**, *309*, 897–903.
- Kou, A.; Gulbis, J. M.; Antcliff, J. F.; Rahman, T.; Lowe, E. D.; Zimmer, J.; Cuthbertson, J.; Ashcroft, F. M.; Ezaki, T.; Doyle, D. A. Crystal structure of the potassium channel KirBac1.1 in the closed state. *Science* **2003**, *330*, 1921–1926.
- Roux, B.; MacKinnon, R. The cavity and pore helices in the KcsA K⁺ channel: electrostatic stabilization of monovalent cations. *Science* **1999**, *285*, 100–103.
- Holyoake, J.; Domene, C.; Bright, J. N.; Sansom, M. S. P. KcsA closed and open: modeling and simulation studies. *Eur. Biophys. J.* **2004**, *33*, 238–246.
- Service, R. F. A new portrait puts potassium pore in a fresh light. *Science* **2005**, *309*, 867.
- Lu, Z.; Klem, A. M.; Ramu, Y. Ion conduction pore is conserved among potassium channels. *Nature* **2001**, *413*, 809–813.
- Schneider, G.; Böhm, H. J. Virtual screening and fast automated docking methods. *Drug Discovery Today* **2002**, *7*, 64–70.
- Oprea, T. I.; Matter, H. Integrating virtual screening in lead discovery. *Curr. Opin. Chem. Biol.* **2004**, *8*, 349–358.
- Doman, T. N.; McGovern, S. L.; Witherbee, B. J.; Kasten, T. P.; Kurumbail, R.; Stallings, W. C.; Connolly, D. T.; Shoichet, B. K. Molecular docking and high-throughput screening for novel inhibitors of protein tyrosine phosphatase-1B. *J. Med. Chem.* **2002**, *45*, 2213–2221.
- Westerfors, M.; Tedebark, U.; Andersson, H. O.; Öhrman, S.; Choudhury, D.; Ersoy, O.; Shinohara, Y.; Axén, A.; Carredano, E.; Baumann, H. Structure-based discovery of a new affinity ligand to pancreatic α-amylase. *J. Mol. Recognit.* **2003**, *16*, 396–405.
- Florianio, W. B.; Vaidehi, N.; Zamanakos, G.; Goddard, W. A., III. HierVLS hierarchical docking protocol for virtual ligand screening of large-molecule databases. *J. Med. Chem.* **2004**, *47*, 56–71.
- Wang, J. L.; Liu, D. X.; Zhang, Z. J.; Shan, S.; Han, X. B.; Srinivasula, S. M.; Croce, C. M.; Alnemri, E. S.; Huang, Z. W. Structure-based discovery of an organic compound that binds Bcl-2 protein and induces apoptosis of tumor cells. *Proc. Natl. Acad. Sci. U.S.A.* **2000**, *97*, 7124–7129.
- Liu, H.; Li, Y.; Song, M.; Tan, X.; Cheng, F.; Zheng, S.; Shen, J.; Luo, X.; Ji, R.; Yue, J.; Hu, G.; Jiang, H.; Chen, K. Structure-based discovery of potassium channel blockers from natural products: virtual screening and electrophysiological assay testing. *Chem. Biol.* **2003**, *10*, 1103–1113.
- Available Chemicals Directory Compound Database; MDL Information Systems, Inc., 2003 (<http://www.mdll.com>).
- (a) Ewing, T.; Kuntz, I. D. Critical evaluation of search algorithms for automated molecular docking and database screening. *J. Comput. Chem.* **1997**, *18*, 1175–1189. (b) Kuntz, I. D. Structure-based strategies for drug design discovery. *Science* **1992**, *257*, 1078–1082.
- Zheng, S.; Luo, X.; Chen, G.; Zhu, W.; Shen, J.; Chen, K.; Jiang, H. A new rapid and effective chemistry space filter in recognizing a druglike database. *J. Chem. Inf. Model.* **2005**, *45*, 856–862.
- Wang, R. X.; Lai, L. H. Calculating partition coefficients of peptides by the addition method. *J. Chem. Inf. Comput. Sci.* **1997**, *37*, 615–621.
- (a) Srinivasan, J.; Cheatham, T. E.; Cieplak, P.; Kollman, P. A.; Case, D. A. Continuum solvent studies of the stability of DNA, RNA, and phosphoramidate–DNA helices. *J. Am. Chem. Soc.* **1998**, *120*, 9401–9409. (b) Massova, I.; Kollman, P. A. Computational alanine scanning to probe protein–protein interactions: a novel approach to evaluate binding free energies. *J. Am. Chem. Soc.* **1999**, *121*, 8133–8143. (c) Chong, L. T.; Duan, Y.; Wang, L.; Massova, I.; Kollman, P. A. Molecular dynamics and free-energy calculations applied to affinity maturation in antibody 48G7. *Proc. Natl. Acad. Sci. U.S.A.* **1999**, *96*, 14330–14335. (d) Gohlke, H.; Case, D. A. Converging free energy estimates: MM-PB(GB)SA studies on the protein–protein complex Ras–Raf. *J. Comput. Chem.* **2004**, *25*, 238–250. (e) Luo, C.; Luo, H.; Zheng, S.; Gui, C.; Yue, L.; et al. Nucleocapsid protein of SARS coronavirus tightly binds to human cyclophilin A. *Biochem. Biophys. Res. Commun.* **2004**, *321*, 557–565.
- GCG, Wisconsin Package, PileUp, version 10.0; Genetics Computer Group: Madison, WI, 2000.
- Insighill, version 2000; Accelrys Molecular Simulations Inc.: San Diego, CA, 2000.
- Weiner, S. J.; Kollman, P. A.; Nguyen, D. T.; Case, D. A. An all-atom force field for simulations of proteins and nucleic acids. *J. Comput. Chem.* **1986**, *7*, 230–252.
- Sybyl, version 6.7; Tripos Associates: St. Louis, MO, 2000.
- Gasteiger, J.; Marsili, M. Iterative partial equalization of orbital electronegativity. A rapid access to atomic charges. *Tetrahedron* **1980**, *36*, 3219–3228.
- (a) Morris, G. M.; Goodsell, D. S.; Huey, R.; Olson, A. J. Distributed automated docking of flexible ligands to protein: parallel application of AutoDock 2.4. *J. Comput.-Aided Mol. Des.* **1996**, *10*, 293–304. (b) Morris, G. M.; Goodsell, D. S.; Halliday, R. S.; Huey, R.; Hart, W. E.; Belew, R. K.; Olson, A. J. Automated docking using Lamarckian genetic algorithm and empirical binding free energy function. *J. Comput. Chem.* **1998**, *19*, 1639–1662.
- Jorgensen, W. L.; Chandrasekhar, J.; Madura, J. D.; Impey, R. W.; Klein, M. L. Comparison of simple potential functions for simulating liquid water. *J. Chem. Phys.* **1983**, *79*, 926–935.
- Case, D. A.; Pearlman, D. A.; Caldwell, J. W.; Cheatham, T. E., III; Wang, J.; Ross, W. S.; Simmerling, C.; Darden, T.; Merz, K. M.; Stanton, R. V.; Cheng, A.; Vincent, J. J.; Crowley, M.; Tsui, V.; Gohlke, H.; Radmer, R.; Duan, Y.; Pitner, J.; Massova, I. *AMBER 7*; University of California: San Francisco, CA, 2002.
- Cornell, W. D.; Cieplak, P.; Bayly, C. I.; Gould, I. R.; Merz, K. M.; Ferguson, D. M.; Spellmeyer, D. C.; Fox, T.; Caldwell, J. W.; Kollman, P. A. A second generation force field for the simulation of proteins, nucleic acids, and organic molecules. *J. Am. Chem. Soc.* **1995**, *117*, 5179–5197.
- Wang, J.; Wolf, R. M.; Caldwell, J. W.; Kollman, P. A.; Case, D. A. Development and testing of a general AMBER force field. *J. Comput. Chem.* **2004**, *25*, 1157–1174.
- Cieplak, P.; Bayly, C. I.; Cornell, W. D.; Kollman, P. A. Application of the multimolecule and multiconformational RESP methodology to biopolymers: Charge derivation for DNA, RNA, and proteins. *J. Comput. Chem.* **1995**, *16*, 1357–1377.
- (a) Onufriev, A.; Bashford, D.; Case, D. A. Modification of the generalized Born model suitable for macromolecules. *J. Phys. Chem. B* **2000**, *104*, 3712–3720. (b) Lee, M. S.; Salsbury, F. R.; Brooks,

- C. L. Novel generalized Born methods. *J. Chem. Phys.* **2002**, *116*, 10606–10614.
- (41) (a) Hermann, R. B. Theory of hydrophobic bonding. II. Correlation of hydrocarbon solubility in water with solvent cavity surface area. *J. Phys. Chem.* **1971**, *76*, 2754–2759. (b) Nozaki, Y.; Tanford, C. The solubility of amino acids and two glycine peptides in aqueous ethanol and dioxane solutions: establishment of a hydrophobicity scale. *J. Biol. Chem.* **1971**, *246*, 2211–2217.
- (42) Sanner, M. F.; Olson, A. J.; Spehner, J. C. Reduced surface: An efficient way to compute molecular surfaces. *Biopolymers* **1996**, *38*, 305–320.
- (43) Song, M. K.; Liu, H.; Jiang, H. L.; Yue, J. M.; Hu, G. Y. Electrophysiological characterization of 14-benzoyletatsamine, a selective blocker of the delayed rectifier K⁺ channel found in virtual screening. *Eur. J. Pharmacol.* **2006**, *531*, 47–53.
- (44) Hu, G. Y.; Biro, Z.; Hill, R. H.; Grillner, S. Intracellular QX-314 causes depression of membrane potential oscillations in lamprey spinal neurons during fictive locomotion. *J. Neurophysiol.* **2002**, *87*, 2676–2883.
- (45) MacKinnon, R.; Cohen, L.; Kuo, A.; Lee, A.; Chait, B. T. Structural conservation in prokaryotic and eukaryotic potassium channels. *Science* **1998**, *280*, 106–109.
- (46) *MDL Drug Data Report (MDDR) Database*; MDL Information Systems, Inc.: San Leandro, CA, 2001.
- (47) Klee, R.; Ficker, E.; Heinemann, U. Comparison of voltage-dependent potassium currents in rat pyramidal neurons acutely isolated from hippocampal regions CA1 and CA3. *J. Neurophysiol.* **1995**, *74*, 1982–1995.
- (48) Numann, R. E.; Wadman, W. J.; Wong, R. K. S. Outward currents of single hippocampal cells obtained from the adult guinea-pig. *J. Physiol.* **1987**, *393*, 331–353.
- (49) (a) Rauer, H.; Grissmer, S. Evidence for an internal phenylalkylamine action on the voltage-gated potassium channel KV1.3. *Mol. Pharmacol.* **1996**, *50*, 1625–1634. (b) Rauer, H.; Grissmer, S. The effect of deep pore mutations on the action of phenylalkylamines on the Kv1.3 potassium channel. *Br. J. Pharmacol.* **1999**, *127*, 1065–1074.
- (50) *PyMOL*, version 0.97; Delano Scientific LLC: San Carlos, CA, 2004 (www.pymol.org).
- (51) *Origin*, version 6.0; Microcal, LLC: Northampton, MA, 1999 (www.microcal.com).
- (52) Wallace, A. C.; Laskowski, R. A.; Thornton, J. M. LIGPLOT: A program to generate schematic diagrams of protein–ligand interactions. *Protein Eng.* **1995**, *8*, 127–134.

JM060414O